Comparative Biochemistry and Physiology - Part D: Genomics and Proteomics 57 (2026) 101672

Contents lists available at ScienceDirect

Comparative Biochemistry and Physiology - Part D: Genomics and Proteomics

journal homepage: www.elsevier.com/locate/cbpd

Transcriptomic and physiological responses of rainbow trout (*Oncorhynchus mykiss*) gill tissues to hypoxic stress

Ziyi Zhao, Mengqun Liu, Qiusheng Wang, Haishen Wen, Xin Qi *

Key Laboratory of Mariculture, Ministry of Education (KLMME), Ocean University of China, Qingdao, 266003, China

ARTICLE INFO

Edited by Chris Martyniuk

Keywords:
Oncorhynchus mykiss
Hypoxic stress
RNA sequencing
Histopathological analysis
Biochemical analysis

ABSTRACT

Hypoxic stress poses a significant challenge to aquaculture productivity. As a hypoxia-intolerant species, rainbow trout (*Oncorhynchus mykiss*) requires further investigation regarding their molecular and physiological adaptations to prolonged hypoxia. In this study, we investigated the temporal dynamics of the hypoxic response in rainbow trout gill cells through an integrated analysis of transcriptomics, histopathology, and biochemical analysis. Primary gill cells exposed to hypoxic conditions (3 % O_2) for 0, 24, and 48 h exhibited a progressive increase in reactive oxygen species (ROS) levels. A total of 6744 differentially expressed genes (DEGs) were identified through RNA sequencing, with the Glycolysis/Gluconeogenesis and Biosynthesis of amino acids pathways significantly upregulated at both 24 and 48 h, indicating a metabolic shift toward anaerobic energy production and antioxidant defense. In contrast, steroid biosynthesis was enriched at 48 h, potentially supporting membrane repair and cortisol-mediated stress adaptation, whereas apoptosis transitioned from inhibition at 24 h to activation at 48 h, correlating with irreversible cellular damage. Weighted Gene Co-expression Network Analysis (WGCNA) identified the module most associated with 48-h hypoxia, which was also enriched in these four pathways. Histopathological and physiological indicators also proved time-dependent changes in tissues upon hypoxic stress. These findings indicated that during early hypoxia (24 h), metabolic adaptation, including Glycolysis/Gluconeogenesis and Biosynthesis of amino acids, was prioritized in rainbow trout. However, after 48 h of hypoxia, a transition from metabolic adaptation to apoptosis-mediated cell clearance was induced, accompanied by the upregulation of steroid biosynthesis to mitigate sustained oxidative damage.

1. Introduction

As a fundamental environmental factor, dissolved oxygen (DO) is crucial for regulating the growth, metabolism, and physiological processes of aquatic animals (Shang et al., 2022). Since at least the mid-20th century, DO concentrations in both marine and freshwater systems have been consistently declining, primarily due to the combined effects of global warming, algal blooms, and tidal cycles. As a result, hypoxic zones have emerged and become increasingly widespread across aquatic ecosystems (Chen et al., 2007; Stramma et al., 2008). When aquatic organisms are exposed to hypoxic conditions, they undergo significant biochemical and physiological changes, affecting various aspects such as growth, development, metabolism, and antioxidant activity (Wilhelm Filho et al., 2005). As a vital organ for gas exchange and respiratory regulation, the gills are highly sensitive to changes in the aquatic environment and play a crucial role in fish adaptation to external conditions (Cappello et al., 2015). When exposed to hypoxic conditions, the normal functions of fish gills may be impaired, leading to pathological changes such as swelling, hypertrophy, hyperplasia, and tissue necrosis (Sollid et al., 2005; Harper and Wolf, 2009; Matey et al., 2011). Studies on *Marsupenaeus japonicus* have demonstrated that hypoxic stress significantly induces apoptosis in the gills and hepatopancreas, leading to pronounced tissue damage (Wang et al., 2022). Acute hypoxia triggers lamellar remodeling, enhanced apoptosis, and elevated antioxidant enzyme activity in the gills of scaleless carp (*Gymnocypris przewalskii*) (Chen et al., 2022). In contrast, rainbow trout, a relatively hypoxia-sensitive species with a lethal threshold of approximately 3 mg/L, tends to exhibit gill injury at earlier stages, showing a staged transition from metabolic adjustment to apoptosis. Therefore, elucidating the hypoxia-induced molecular responses and adaptive mechanisms in gill tissues of rainbow trout is critical for understanding aquatic species' survival strategies in oxygen-depleted environments, which holds significant implications for both aquaculture conservation and ecological management under escalating hypoxic challenges.

* Corresponding author.
E-mail address: qx@ouc.edu.cn (X. Qi).

https://doi.org/10.1016/j.cbd.2025.101672
Received 4 September 2025; Received in revised form 28 October 2025; Accepted 28 October 2025
Available online 30 October 2025

The balance of ROS in fish is regulated by the antioxidant defense system, which maintains redox equilibrium (Qiang et al., 2013; Schulte, 2015). Under hypoxic stress, to preserve homeostasis and mitigate ROS-induced damage, the antioxidant system enhances the production of antioxidant enzymes such as SOD and CAT. This adaptive response contributes to improved hypoxia tolerance (Cheng et al., 2018). As the first line of defense in the antioxidant system (Mruk et al., 2002), the enzyme SOD catalyzes the conversion of O_2^- into hydrogen peroxide (H_2O_2) and oxygen (O_2), protecting organisms from ROS-induced damage (He et al., 2016). To mitigate oxidative stress, CAT scavenges hydrogen peroxide by catalyzing its decomposition into water and oxygen, thereby protecting cells from oxidative damage (Zelko et al., 2002). Under hypoxic stress, Liang et al. observed elevated activities of SOD, CAT, MDA, and GSH in *Megalobrama amblycephala* gills compared to normoxic controls (Shuang et al., 2022). In contrast, after 12 h of hypoxic stress, both the levels and activities of Gpx, CAT, SOD, and MDA in largemouth bass (*Micropterus salmoides*)showed a significant decreasing trend (Yang et al., 2017). Overall, these findings indicate that hypoxic stress disrupts oxidative balance in fish and modulates antioxidant enzyme activity. The severity and duration of hypoxia exert species- and tissue-specific effects on oxidative defense mechanisms. Prolonged oxidative stress disrupts cellular homeostasis while simultaneously acting as a key trigger for apoptosis, ultimately resulting in tissue dysfunction and damage (Liu et al., 2023).

The transcriptional response mechanisms to hypoxia have been extensively investigated in the gills of various teleost species. In the hypoxia study of *Sillago sihama*, transcriptomic responses in gill tissues were analyzed across different durations of hypoxic exposure. DEGs commonly identified across all treatment groups were significantly enriched in pathways related to steroid biosynthesis, amino acid biosynthesis, glutathione metabolism, ferroptosis (Saetan et al., 2020). Studies indicate that in largemouth bass (*M. salmoides*), 96 h of acute hypoxic stress activates pathways related to antioxidant defense, apoptosis, and inflammation, with the MAPK signaling pathway serving as a key regulator in the hypoxic response (Song et al., 2022). To investigate the response of *Takifugu obscurus* to acute hypoxic stress, a transcriptomic analysis based on high-throughput sequencing was conducted to evaluate the gill response of *T. obscurus* to such stress. The results indicated that most DEGs in the gills under hypoxic stress were primarily involved in immune responses, while a smaller subset participated in cell growth and development, angiogenesis, and apoptotic processes (Zhang et al., 2023). Overall, transcriptomic analysis provided critical insights into the molecular mechanisms regulating key biological processes in fish under hypoxic stress, including oxidative stress, anaerobic energy metabolism, and programmed cell death. Investigating the transcriptional responses of fish gills to hypoxia offers valuable understanding of their adaptive strategies for survival in low-oxygen environments.

As a commercially valuable cold-water species, rainbow trout (*Oncorhynchus mykiss*) is widely cultivated worldwide. With a lethal hypoxia threshold of 3 mg/L, *O. mykiss* exhibits higher sensitivity to low oxygen than most fish species, making it a valuable model for hypoxic stress research (Hou et al., 2020). Due to several negative factors, such as global warming and eutrophication, which affect oxygen levels in water, commercially valuable trout species, particularly *O. mykiss*, are facing significant threats (Aksakal et al., 2023). Thus, exploring the molecular mechanisms underlying hypoxic stress in rainbow trout is essential for optimizing aquaculture conditions. Currently, research on hypoxic stress in rainbow trout primarily focuses on the organismal level, while studies at the cellular level remain limited. In this study, rainbow trout gill cells were exposed to hypoxic stress for varying durations to evaluate oxidative stress responses and to identify differentially expressed genes and key biological pathways associated with hypoxia adaptation using RNA-Seq. Additionally, the physiological and histological responses to acute hypoxia were examined at the individual level. Collectively, these findings provide an effective approach for understanding hypoxia adaptation in rainbow trout and may contribute to the selective breeding of hypoxia-tolerant fish.

2. Materials and methods

2.1. Experimental animals

Healthy rainbow trout (~15 g, ~10 cm), were obtained from a breeding farm in Weifang, Shandong. A total of 120 fish were randomly selected and temporarily housed in 10 tanks. During the acclimation period, the fish were maintained in aerated tap water for 24 h. Water temperature was controlled between 16 and 18 °C, with dissolved oxygen levels maintained at approximately 8 mg/L to minimize the influence of farm-specific environmental factors. The fish were fed twice daily, and any uneaten feed and feces were removed using a siphon. Feeding was discontinued 24 h before the start of the experimental treatments. All animal experiments were conducted in accordance with the guidelines of the Animal Research and Ethics Committee of Ocean University of China (Permit Number: 20141201). The species involved in this study are neither protected nor classified as endangered.

2.2. Determination of DO in hypoxic experiment

To assess hypoxia tolerance at both the individual and cellular levels, a preliminary experiment was conducted prior to the formal study. First, two tanks were randomly selected, and the aeration system was turned off to gradually deplete dissolved oxygen, which was continuously monitored in real-time using an EcoSense DO200A (YSI, USA). When dissolved oxygen levels reached 3 ± 0.2 mg/L, the trout exhibited surface air-gulping behavior, known as “floating head.” This observation guided the selection of 3 mg/L as the hypoxic condition for subsequent individual-level experiments to ensure normal survival. Notably, this DO level is also widely adopted as a hypoxic condition in studies of other fish species, including largemouth bass, scaleless carp, zebrafish, killifish, and Nile tilapia (Stierhoff et al., 2003; Tran-Duy et al., 2008; Feng et al., 2016; Sun et al., 2020; Chen et al., 2022). Four healthy rainbow trout were selected for primary gill cell culture, and the cells were exposed to different oxygen concentrations (5 % O_2, 3 % O_2, and 1 % O_2) in a cell incubator (Smarter118, USA) during the preliminary experiment. Cell viability was assessed using the Trypan Blue exclusion method, in which equal volumes of cell suspension and 0.4 % Trypan Blue solution (1:1) were mixed, incubated for 3 min at room temperature, and counted on a hemocytometer under a light microscope. The 3 % O_2 group exhibited a moderate survival rate, indicating it as the most suitable hypoxic concentration. Consequently, this concentration was chosen as the hypoxic condition for subsequent cellular experiments. For sampling times, we used two predefined quality-control checkpoints: 24 h, when behavioral indices had stabilized without mortality, and 48 h, when stress became sustained yet remained within welfare limits. Accordingly, all downstream assays sampled at 24 h and 48 h under 3 ± 0.2 mg/L DO (fish) and 3 % O_2 (cells). These two time points were also consistent with previous hypoxia studies in teleosts, which commonly employed 24 h and 48 h exposures to represent early adaptive and prolonged stress phases (Roesner et al., 2006; Mu et al., 2020; Xing et al., 2025).

2.3. Hypoxia treatment and sampling at individual level and cellular level

The hypoxic and control groups were each assigned to three tanks. Normoxic controls were maintained under ambient oxygen, while the hypoxic group underwent acute oxygen reduction to 3.0 ± 0.5 mg/L via nitrogen injection with sustained hypoxic exposure. Samples were collected at 0, 24, and 48 h post-hypoxia and the groups were designated as DH0h, DH24h, and DH48h, respectively. At each sampling point, five fish per tank were randomly selected, anesthetized with MS-222, and gill tissue samples were dissected and divided into three portions: one was

rapidly flash-frozen in liquid nitrogen for storage at −80 °C for molecular analysis, one was fixed in 4 % formaldehyde and subsequently preserved in 70 % ethanol for histological analysis, and one was fixed in 2.5 % glutaraldehyde for ultrastructural analysis.

Eighteen rainbow trout were randomly selected from the remaining normoxic tanks for primary gill cell culture. After excision, the branchial arches were removed, and the remaining gill filaments were used to establish primary cultures comprising mixed gill cells. After obtaining the gill tissue, it was rinsed three times in phosphate-buffered saline (PBS) supplemented with 1 % penicillin-streptomycin-amphotericin B. The tissue was then minced and digested with trypsin for 20 min, followed by centrifugation (500 ×*g*, 5 min) to remove the supernatant. The cell suspension was filtered through sterile 40 μm cell strainers and resuspended. After seeding in 6-well plates, cells were incubated at 16 °C for 24 h in M199 complete medium containing 20 % fetal bovine serum (FBS) and 1 % penicillin-streptomycin-gentamicin (Absin, Shanghai, China). They were then incubated under 3 % O_2 for 24 h and 48 h, with 0 h serving as the normoxic control (DH0h). Upon completion of the hypoxic treatment, cells were immediately harvested, with one portion allocated for reactive oxygen species (ROS) assays and the other for RNA extraction.

2.4. Detection of ROS

ROS production was measured using ROS assay kits (Nanjing Jiancheng, China). The appropriate concentration of the DCFH-DA probe was added to hypoxia-treated cells, followed by incubation at 37 °C for 20 min. The cells were then washed repeatedly with 0.01 M PBS. ROS generation was observed using the green fluorescence channel of fluorescence microscope (Echo Revolve, USA), and fluorescence intensity was quantified using ImageJ (Schneider et al., 2012).

2.5. RNA extraction and RNA-Seq library construction and sequencing

Gill cell RNA was extracted using RNAiso reagent (Takara, Otsu, Japan). Concentration was quantified with a NanoDrop 2000 spectrophotometer (Thermo Scientific, Waltham, MA), and RNA quality was evaluated using an Agilent 2100 Bioanalyzer. Sequencing libraries for 18 gill cell samples (three treatment groups with six replicates each) were then prepared and sequenced on the Illumina HiSeq X Ten platform, generating 150 bp paired-end reads. The raw sequencing data were submitted to the NCBI SRA database.

2.6. Identification and functional enrichment analysis of DEGs

Quality control of raw sequencing reads was performed using FastQC v0.11.9 (Ward et al., 2020). Subsequently, Trimmomatic v0.38 (Bolger et al., 2014) was subsequently used to trim adapter sequences, remove poly-N stretches, and filter out low-quality reads (average Q-score < 20), yielding high-quality clean reads. These reads were mapped to the *Oncorhynchus mykiss* reference genome (GCA_013265735.3) via HISAT2 (Gill and Dhillon, 2022). Gene expression levels were quantified by counting reads aligned to coding sequences (CDS) with featureCounts v2.0.1 (Liao et al., 2014), and FPKM values were estimated using StringTie v2.1.6 (Pertea et al., 2015). Differentially expressed genes (DEGs) were identified using the DESeq2 R package v1.30.0, with the criteria of $|\log_2$ fold change (FC)$| \geq 1$ and p-value < 0.05. Principal component analysis (PCA) was performed to evaluate the reliability of biological replicates and assess variations between different samples.

To explore the biological functions of DEGs under hypoxic treatment, Gene Ontology (GO) and Kyoto Encyclopedia of Genes and Genomes (KEGG) enrichment analyses were conducted using KOBAS (http://bioinfo.org/kobas) with a significance threshold of p-value < 0.05. The resulting enrichment data were visualized using an online platform Weishengxin (https://www.bioinformatics.com.cn/).

2.7. Co-expression network and hub genes analysis

Using the Weighted Gene Co-expression Network Analysis (WGCNA) v1.46 R package (Langfelder and Horvath, 2008), genes with FPKM < 1 were filtered out before constructing a weighted gene co-expression network. Co-expression modules were built using an unsigned topology model with a soft threshold of 12, a minimum module size of 100, and a cut height of 0.25. Module identification was performed using the tree-cut algorithm. The correlation between module eigengenes and each experimental group was evaluated using Pearson's correlation test, with only modules showing a p-value < 0.05 considered significantly associated with the hypoxia group. The module showing the highest correlation with the 48-h hypoxic treatment was selected for further analysis. Protein sequences from the blue module were extracted, and their targeting relationships were predicted using STRING software. Genes within the module with a WGCNA edge >0.3 were analyzed using Cytoscape 3.8.1 (Shannon et al., 2003), and hub genes were identified based on their connectivity degree, as determined by CytoHubba (Chin et al., 2014).

2.8. Real-time quantitative PCR (qPCR) validation

Seven genes including *gadd45ba*, *ga45b*, *bcl2l1*, *tuba1a*, *aldocb*, arg*2*, *cbsb*, and reference gene (18s RNA) were selected for qPCR analysis to validate the accuracy of the sequencing data, with specific primers designed using NCBI (https://www.ncbi.nlm.nih.gov/tools/primer-blast/) (Table S1). Total RNA of primary gill cell from sequencing samples was reverse transcribed into cDNA using MonScript™ RTIII Super Mix with dsDNase (Vazyme, Nanjing, China). qPCR was performed on an Applied Biosystems 7300 system (Applied Biosystems, Foster, CA, USA) using the SYBR-Green kit. The reaction mixture contained 5 μL ChamQ™ SYBR Color qPCR Master Mix (Vazyme, Nanjing, China), 3.6 μL nuclease-free water, 1 μL cDNA, and 0.2 μL of each primer. The amplification protocol included an initial denaturation at 95 °C for 30 s, followed by 40 cycles of 10 s at 95 °C, 30 s at 60 °C, and 30 s at 72 °C. The 18S rRNA gene served as the reference gene. Relative gene expression levels were quantified with three biological and technical replicates, with statistical analysis performed via the $2^{-\Delta\Delta CT}$ method (Livak and Schmittgen, 2001).

2.9. Histopathology and transmission electron microscopy (TEM) analysis

The fixed samples underwent gradient dehydration using ethanol solutions of increasing concentrations. After dehydration, the tissues were cleared with two xylene treatments, infiltrated with molten paraffin wax in an embedding machine, and sectioned into 5 μm thick slices. Apoptosis levels were assessed using the TUNEL BrightGreen Apoptosis Detection Kit (Vazyme, Nanjing, China) following the manufacturer's protocol. Total nuclei were stained with DAPI, appearing blue, while apoptotic cells were labeled with TUNEL, emitting green fluorescence. The double-stained sections were observed and imaged using a laser scanning confocal microscope, and apoptosis was semi-quantitatively analyzed with ImageJ. The apoptotic index was calculated as the average of values from three fields of view. For ultrastructural analysis, glutaraldehyde-fixed tissues were sent to the Qingdao University Medical Science Center (Qingdao, China).

2.10. Measurement of biochemical indicators

The MDA content (Item No. A003-1), SOD activity (Item No. A001-1), and CAT activity (Item No. A007-1-1) were assayed using commercial kits (Nanjing Jiancheng Bioengineering Institute, China) according to the manufacturer's protocols. Following the manufacturer's instructions, the absorbance of the reaction solutions was measured at specific wavelengths using a Biotek Gen 5 microplate reader (Agilent,

USA), and the results were calculated based on the formulas provided in the product manuals.

2.11. Statistical analysis

Biological replicates were defined as independent fish (individual level) or primary gill cell cultures from distinct fish (cellular level). Wells or fields from the same individual were treated as technical replicates. Statistical analyses were performed using one-way ANOVA with Tukey's post hoc and correlation analysis in SPSS v25.0 (Liang et al., 2019). Differences were considered statistically significant at $p < 0.05$. Data are presented as mean ± standard deviation (SD) from three independent biological replicates. Graphs were generated using GraphPad Prism 8.0 (Peivandi et al., 2024).

3. Results

3.1. Effects of hypoxia on ROS levels in rainbow trout gill cells

To examine the effect of hypoxia on ROS levels in rainbow trout gill cells, we exposed the cells to hypoxic conditions for 0, 24, and 48 h. ROS levels were then assessed using a ROS detection kit. As shown in Fig. 1, the intensity of green fluorescence progressively increased with prolonged hypoxic exposure under the same field of view. Quantitative analysis with ImageJ revealed a significant increase in fluorescence intensity at 24 and 48 h compared to the 0-h control group ($p < 0.05$). These findings suggest that prolonged hypoxic stress markedly elevates ROS levels in rainbow trout gill cells.

3.2. Overview of transcriptomic sequencing data

RNA sequencing was performed on 18 gill cell samples collected from rainbow trout subjected to hypoxic treatments for 0, 24, and 48 h, generating 133.34 Gb of raw reads. After filtering, 127.68 Gb of high-quality clean reads were obtained and used for further analysis (PRJNA1270413). The relevant data statistics are presented in Table S2. All samples met the quality criteria of Q20 ≥ 95.83 %, Q30 ≥ 90.10 %, and a GC content exceeding 49.09 %. The total mapping rate of clean reads to the assembled transcriptome ranged from 83.79 % to 96.72 %, with an average of 94.16 %. Principal component analysis (PCA) showed strong clustering among biological replicates, with tight aggregation observed within treatment groups (Fig. 2A), indicating high reproducibility of the transcriptomic profiles.

3.3. Identification of DEGs

A total of 6744 DEGs were identified across three pairwise comparisons: DH0h vs. DH24h, DH0h vs. DH48h, and DH24h vs. DH48h. The analysis primarily focused on the first two comparisons. As shown in Fig. 2B, 387 upregulated genes and 589 downregulated genes were detected in the DH0h vs. DH24h group. In the DH0h vs. DH48h comparison, 2550 genes were upregulated and 2698 were downregulated. To visualize the distribution of DEGs, a corresponding volcano plot was generated (Fig. S1). Accordingly, downstream analyses centered on the two baseline contrasts (DH0h vs. DH24h group and DH0h vs. DH48h group). The DH24h vs. DH48h comparison served as a consistency check, with GO/KEGG enrichments closely matching DH0h–DH48h (Fig. S3).

3.4. Enrichment analysis

GO enrichment analysis classified the DEGs into three categories: molecular functions (MF), biological processes (BP), and cellular components (CC). In the DH0h vs. DH24h comparison (Fig. 3A), hypoxic stress significantly affected functional categories related to cellular respiration and membrane structure, including the mitochondrial respiratory chain complex IV (GO:0005751), oxidoreductase activity (GO:0016491), and membrane (GO:0016020). The downregulation of genes associated with the mitochondrial respiratory chain complex IV suggests a suppression of oxidative phosphorylation. Similarly, the enrichment of membrane-related genes was observed, with most of them being downregulated. In contrast, oxidoreductase activity exhibited

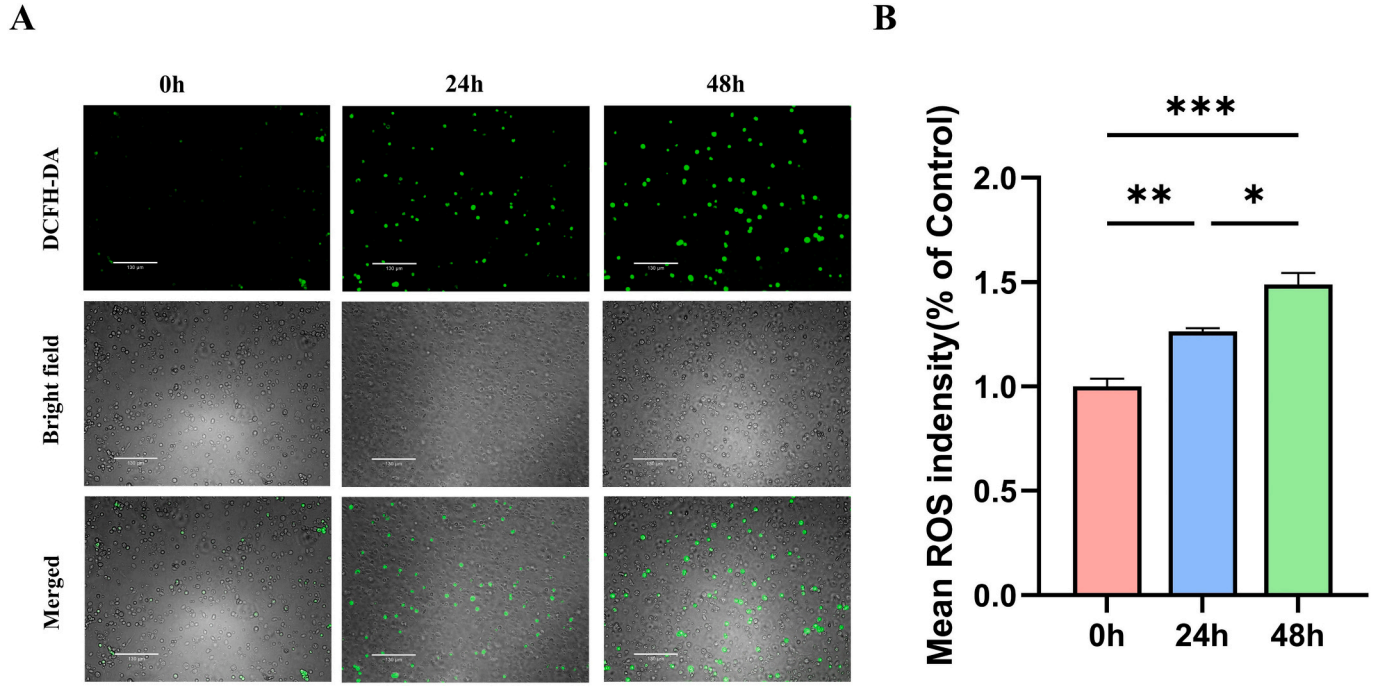

Fig. 1. ROS detection under hypoxic conditions. (A) Representative fluorescence images of ROS detection at 0 h at 21 % O_2, 24 h, and 48 h under 3 % O_2 exposure. The top row shows DCFH-DA fluorescence indicating ROS accumulation, the middle row displays bright field images, and the bottom row shows merged images. Scale bar = 130 μm. (B) Quantification of ROS intensity at 0 h, 24 h, and 48 h, presented as the percentage relative to control (21 % O_2).

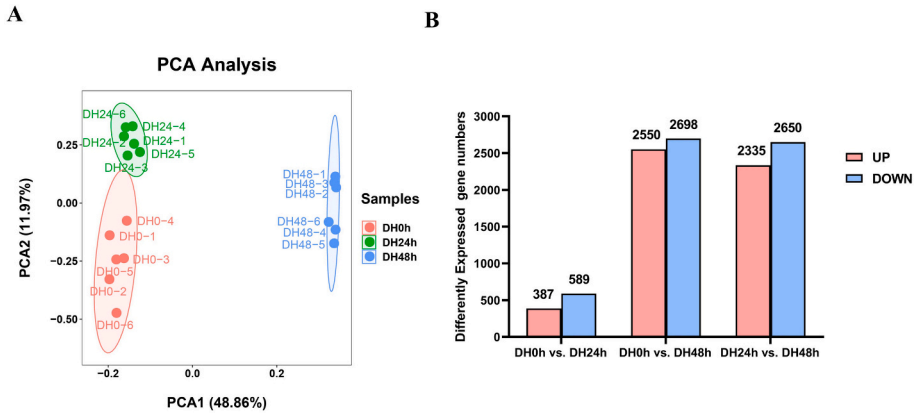

Fig. 2. Bioinformatic analysis of RNA-seq data. (A) The principal component analysis (PCA) plot for three groups (DH0h, DH24h and DH48h). (B) The number of DEGs between DH0h vs. DH24h, DH0h vs. DH48h and DH24h vs. DH48h.

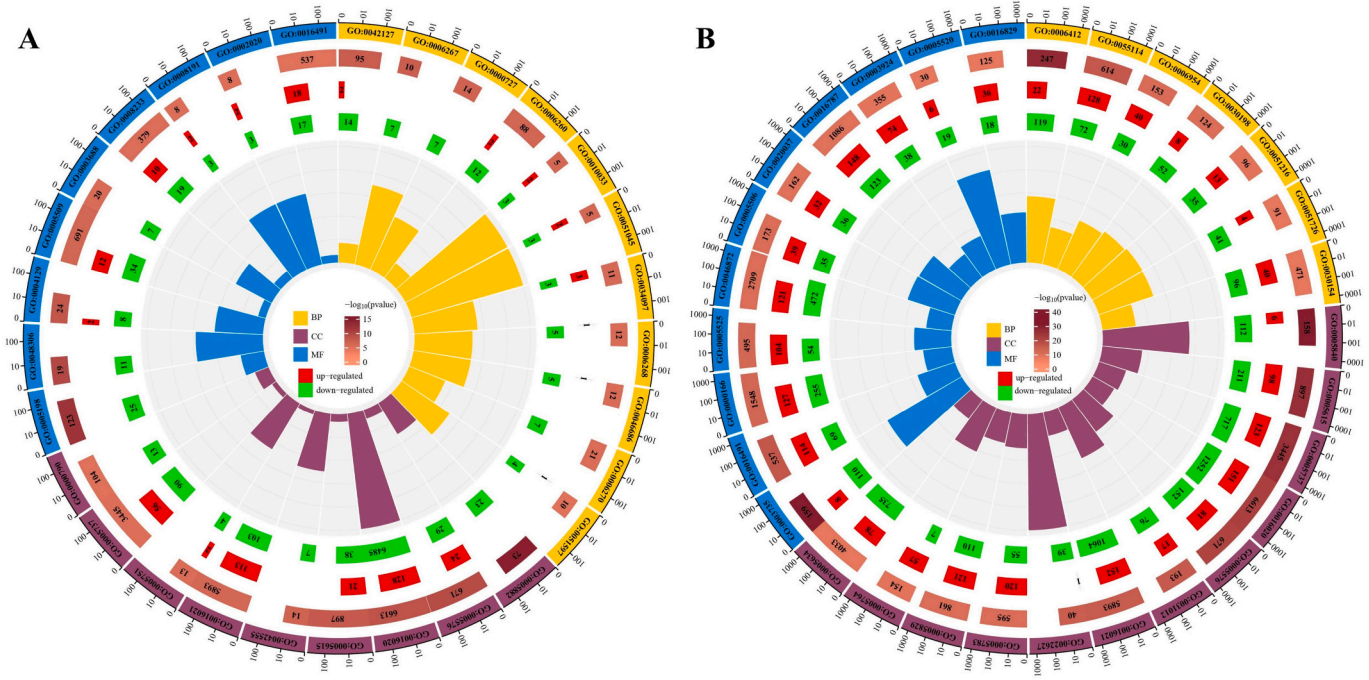

Fig. 3. Top 30 GO enrichment results for (A) DH0h vs. DH24h group and (B) DH0h vs. DH48h group respectively. The bar charts illustrate the significance of enrichment ($-\log_{10}$(*p*-value)) for each GO term, with colors representing the regulatory status of the genes: red for upregulated and green for downregulated genes.

both up- and down-regulated genes, reflecting a dynamic balance between ROS generation and antioxidant defense. After 48 h of hypoxia in DH0h vs. DH48h group (Fig. 3B), GO analysis revealed a stronger response than at 24 h, with immune and energy-related functions, such as inflammatory response (GO: 0006954), lysosome (GO:0005764), and GTP binding (GO:0005525), significantly enriched and dominated by upregulated genes. Oxidoreductase activity, initially balanced at 24 h, became upregulated, suggesting enhanced oxidative stress and antioxidant defense. GO term and corresponding Category & Term were shown in Table. S3.

KEGG enrichment analysis of DEGs at 24 and 48 h of hypoxic stress revealed significant enrichment in multiple pathways, including Glycolysis/Gluconeogenesis, Apoptosis, Biosynthesis of amino acids and Steroid biosynthesis (Fig. 4). In the DH0h vs. DH24h group, DEGs in pathways like Glycolysis/Gluconeogenesis pathway and Biosynthesis of Amino Acids were significantly upregulated, whereas in the Apoptosis pathway was notably downregulated (Fig. 4A, B). In the DH0h vs. DH48h comparison, DEGs in pathways like Glycolysis/Gluconeogenesis pathway and Biosynthesis of Amino Acids remained significantly upregulated. Meanwhile, DEGs in the Apoptosis pathway, which were downregulated at 24 h, became upregulated after 48 h. Additionally, DEGS in the Steroid Biosynthesis pathway were significantly enriched in the DH0h vs. DH48h group (Fig. 4C, D).

3.5. *WGCNA and hub gene identified*

To gain deeper insight into the gene networks associated with hypoxic stress, WGCNA was conducted to identify modules significantly correlated with hypoxic treatment. A total of nine distinct modules were constructed, each represented by a unique color, to analyze modules-traits relationships and identify key modules of interest (Fig. 5A). Given the more pronounced stress responses of gill cells to 48-h hypoxic exposure (Fig. 1), the MEblue module, which exhibited the strongest correlation with the DH48 group, was selected for further analysis. The correlation coefficient between the MEblue module and the DH48h treatment was 0.96 (Fig. 5B).

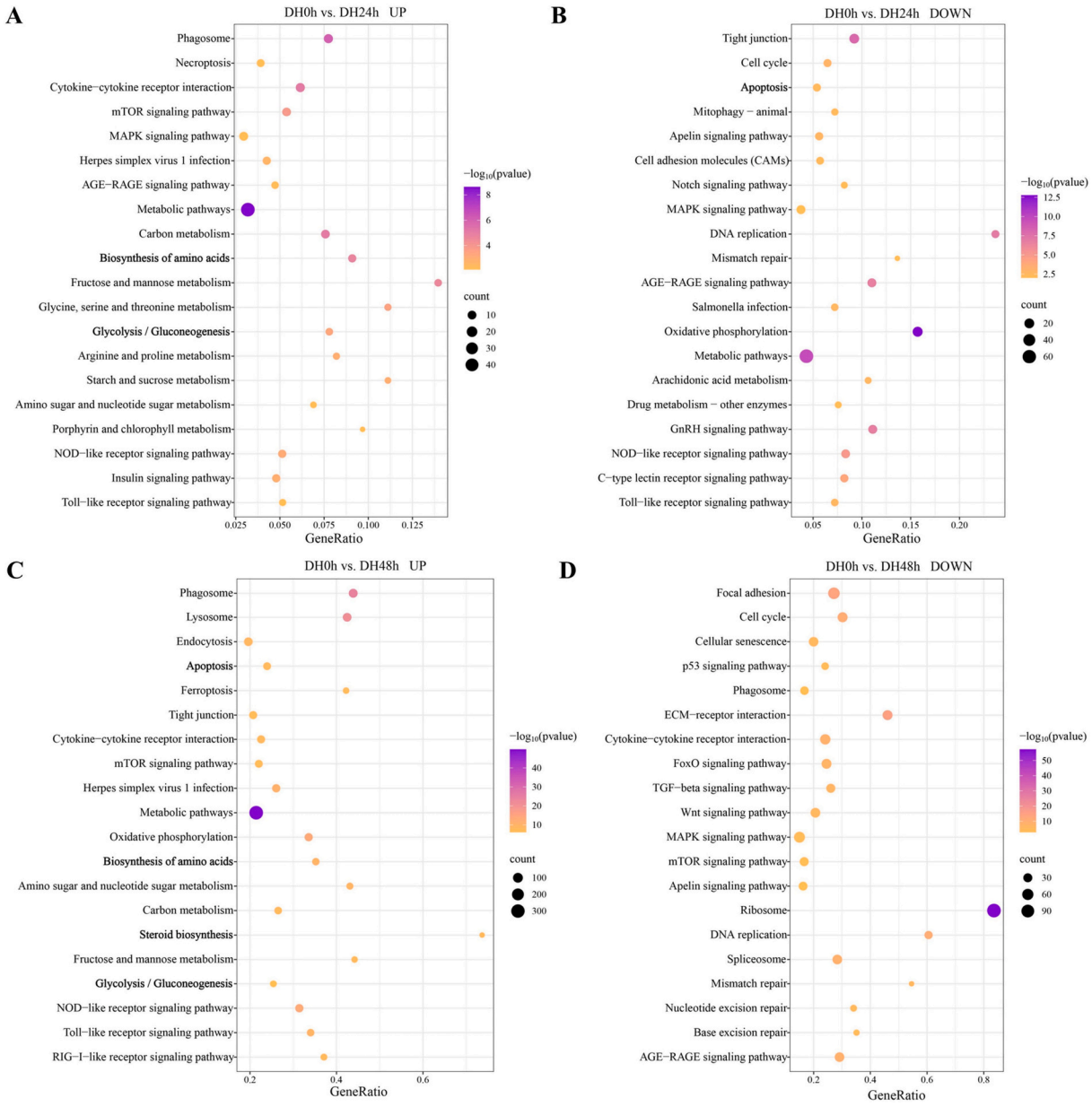

Fig. 4. Top 20 KEGG pathways for DH0h vs. DH24h (A) upregulated, (B) downregulated group, and DH0h vs. DH48h (A) upregulated, (B) downregulated group, respectively.

3.6. PPI network construction and hub genes recognition

As shown in Fig. 6A, a total of 979 genes were assigned to the MEblue module, among which *pgk1*, *gapdhs*, *eprs1*, *eef2b*, *cs*, *actb2*, *yars1*, *ubb*, *sec61a1*, and *rpl3* were identified as hub genes. To further investigate the biological functions of the selected MEblue module under hypoxic stress, GO and KEGG enrichment analyses were conducted. As shown in Fig. 6B, genes in the MEblue module were primarily enriched in GO terms related to oxidative stress and metabolism, including response to hypoxia, peroxidase activity, glycolysis process, and steroid metabolic process. Additionally, KEGG pathway analysis revealed significant enrichment in pathways such as Apoptosis, Glycolysis/Gluconeogenesis, Biosynthesis of amino acids, and Steroid biosynthesis (Fig. 6C). These findings are consistent with the enrichment results of DEGs, further supporting the involvement of the MEblue in hypoxia-induced metabolic and stress responses.

3.7. Differential gene screening and qPCR validation

Based on the results of the MEblue module identified through WGCNA and a literature review on the functional roles of the corresponding DEGs, we found that many genes involved in the four key pathways were significantly induced under hypoxic conditions (Fig. 7). These include: 1) Apoptosis-related genes: *casp6a*, *actb2*, *akt3a*, *gadd45ba*, *map2k2a*, *map3k5*, and *bcl2l1*; 2) Glycolysis/gluconeogenesis-related genes: *pgm1*, *pgm2*, *hk1*, *pfklb*, *aldocb*, *gapdhs*, and *pgk1*; 3) Steroid biosynthesis-related genes: *fdft1*, *lss*, *dhcr7*, *shcr24*, and *tm7sf2* and 4) Biosynthesis of amino acids-related genes: *aldocb*, *pgk1*, *pgam1a*, *bcat2*, *mat2aa*, and *cbsb*. Based on these findings and a thorough literature review, we hypothesize that potential regulatory interactions may exist among several of these genes under hypoxia stress.

Additionally, to validate the credibility of the RNA-Seq, seven genes (*gadd45ba*, *ga45b*, *bcl2l1*, *tuba1a*, *aldocb*, arg2, and *cbsb*) were selected for the qPCR analysis (Fig. S2). The qPCR results exhibited a strong positive correlation with RNA-Seq data, with correlation coefficients R^2

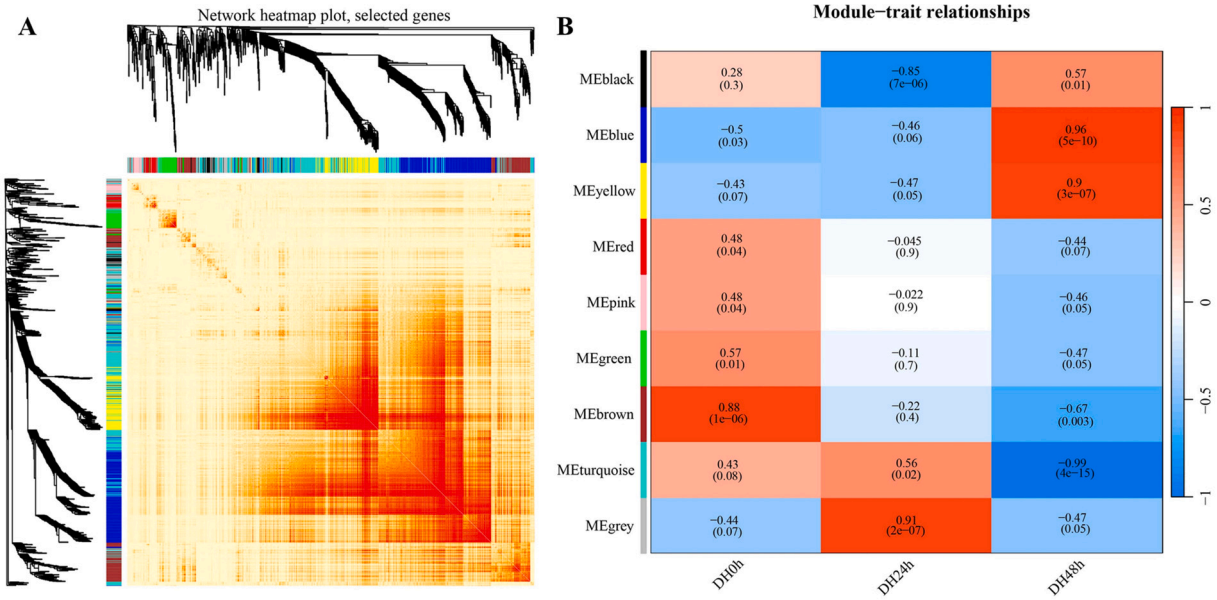

Fig. 5. Modules and regulation networks identified using Weighted Gene Co-expression Network Analysis (WGCNA). (A) Modules identified and different colors represent the corresponding different modules, (B) correlation indices and correlations between different hypoxic treatments and modules.

Fig. 6. PPI network of DEGs and the identified hub genes of WGCNA for (A) blue module. GO enrichment result (B) and KEGG enrichment result (C) for corresponding modules.

> 0.85, confirming the dependability and precision of transcriptome sequencing and analysis.

3.8. Changes in histopathology, ultrastructure, and physiological index

To better understand the gill response to hypoxic stress in rainbow trout, we assessed the effects of hypoxia on the gills at the individual level by examining apoptosis, ultrastructural changes, and physiological index alterations at different time points. TUNEL staining revealed that the number of TUNEL-positive cells (apoptotic cells) progressively increased with the duration of hypoxic stress, resulting in a significantly higher apoptosis index compared to the control group ($p < 0.05$)

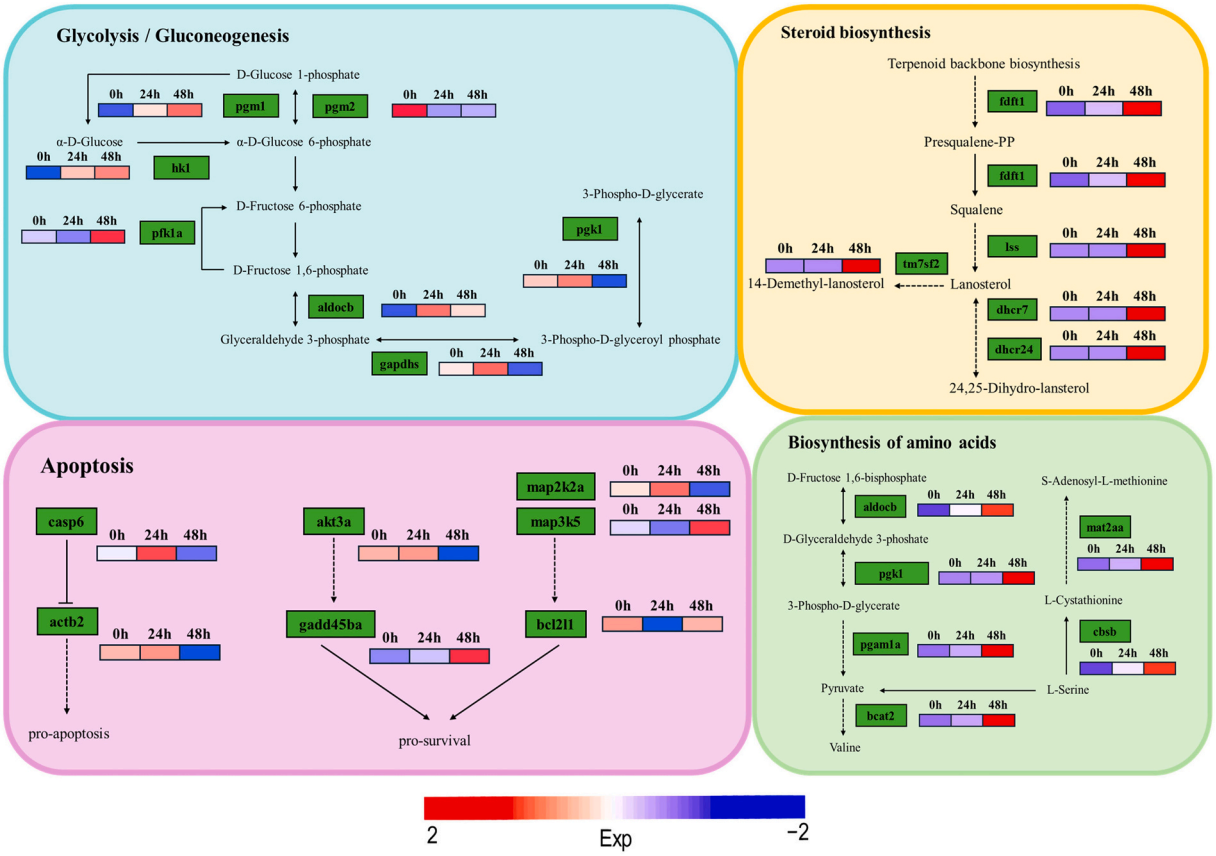

Fig. 7. Genes and pathways affected by different hypoxic treatments in rainbow trout, as determined from transcriptome and pathway enrichment analyses. Pathways are highlighted in grey, and expression patterns of DEGs in different hypoxic comparison groups are represented by the relative expression levels.

(Fig. 8A, B). Meanwhile, TEM analysis showed that mitochondria in gill cells of the normoxic group appeared intact and well-organized. After 24 h of hypoxia, mitochondrial cristae were disrupted, and vacuolization increased. After 48 h of hypoxia, vacuoles ruptured and disappeared, the nuclear membrane was lost, the nucleolus became folded and deformed, and damage to the mitochondrial cristae was further aggravated (Fig. 9). Furthermore, hypoxic stress affected the antioxidant enzyme activity in the gills of rainbow trout (Fig. 10). Under hypoxic conditions, both MDA content and SOD activity significantly increased with prolonged exposure compared to the control group. CAT activity initially increased significantly, peaking at 24 h, and then decreased. These findings suggest that hypoxia activated the enzymatic antioxidant defense system in rainbow trout.

4. Discussion

This study combined transcriptomic and individual-level analyses to reveal a staged hypoxia response in rainbow trout: 0 h represented

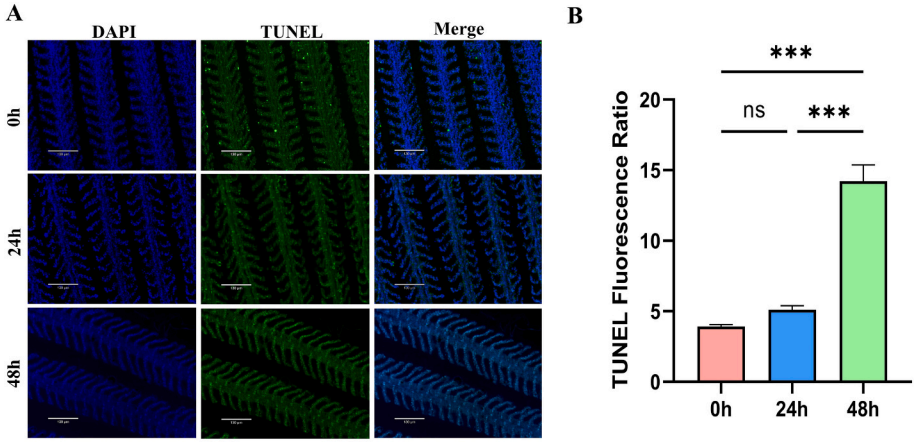

Fig. 8. Apoptosis detection in gills under hypoxic conditions. (A) Representative fluorescence images showing apoptosis detection in gill tissue at 0 h at 21 % O_2, 24 h and 48 h under 3 % O_2 exposure. The left panel shows DAPI staining (blue) for cell nuclei, the middle panel shows TUNEL staining (green) indicating apoptotic cells, and the right panel shows merged images (blue and green). Scale bar = 130 μm. (B) Quantification of apoptosis in gill tissue at 21 % O_2, 24 h and 48 h under 3 % O_2 exposure, expressed as the TUNEL fluorescence ratio (TUNEL/DAPI). A significant difference between groups at $p < 0.05$ is indicated as above.

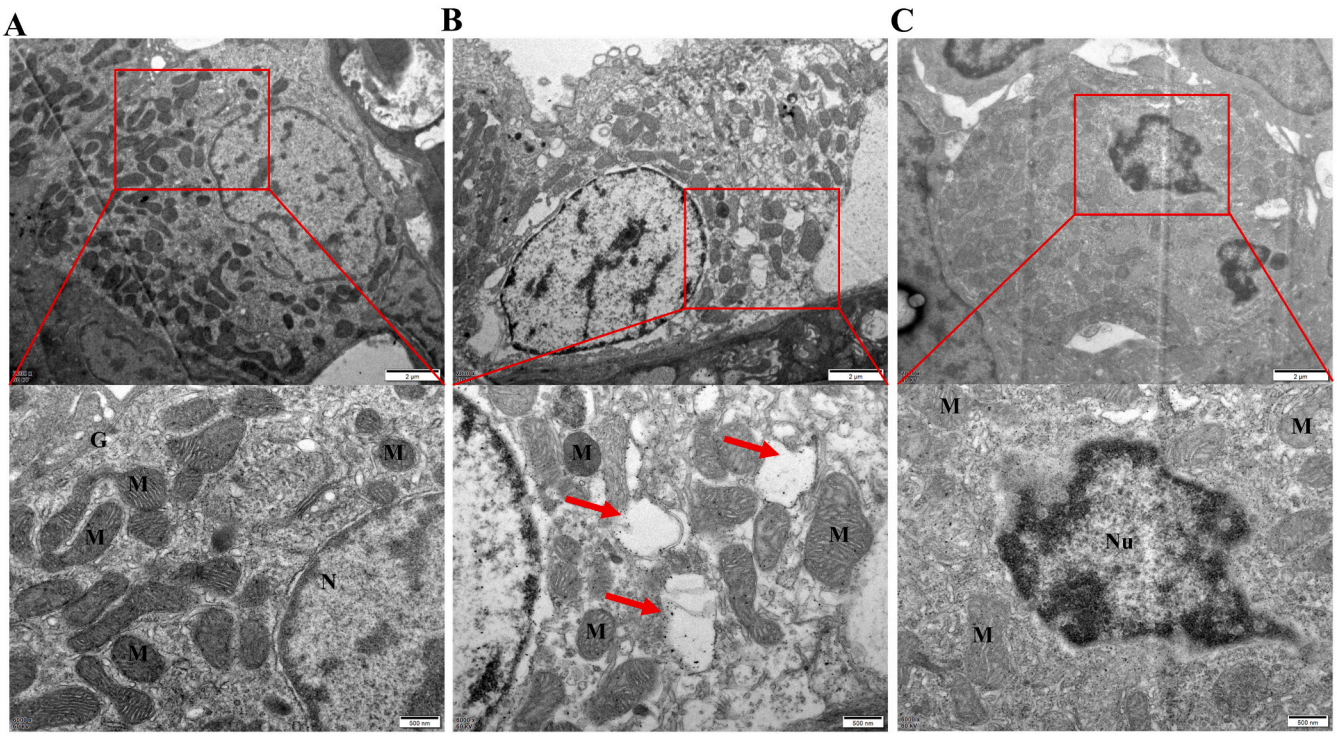

Fig. 9. TEM images in gill tissue of rainbow trout exposed to different hypoxic conditions. (A) Control exposure group; (B) hypoxia for 24 h; (C) hypoxia for 48 h.

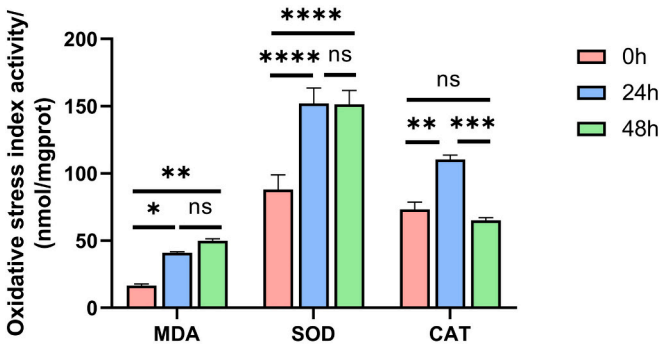

Fig. 10. The physiological indexes of rainbow trout under hypoxia stress: MDA, SOD and CAT. Each bar represents the mean ± SEM (n = 3). A significant difference between groups at $p < 0.05$ is indicated as above.

baseline, 24 h was dominated by metabolic adaptation and antioxidant activation, and 48 h involved structural damage, activation of steroid biosynthesis, and induction of apoptosis. We interpreted the time course within a baseline-anchored, two-phase framework: 0–24 h reflected early adaptation dominated by metabolic reprogramming and redox buffering, whereas 0–48 h represented a late phase characterized by consolidation of these programs together with structural injury and apoptosis. In this framework, the intermediate contrast (DH24h vs. DH48h) served as a consistency check; its GO/KEGG profile mirrored DH0h–DH48h with larger effect sizes, indicating reinforcement rather than redirection of late-phase pathways. Histopathological and physiological readouts (greater tissue injury and oxidative stress at 48 h) converged with the transcriptomic patterns and defined a staged hypoxia response, linking molecular programs to tissue-level phenotypes over time.

4.1. *Hypoxia-induced histopathological alterations in gill of rainbow trout*

Under hypoxic stress, fish tissues and organs inevitably sustain a certain degree of damage. As the primary organ responsible for gas exchange, the gills play a crucial role in oxygen and carbon dioxide exchange, water balance maintenance, and ion regulation (Rombough, 2007; Brauner and Rombough, 2012; Pan and Perry, 2020). Hypoxic stress can induce structural changes in the gills and even impair their function. In grass carp (*Ctenopharyngodon idella*), hypoxic conditions have been reported to cause endoplasmic reticulum dilation and mitochondrial swelling in gill cells (Huang et al., 2024). In largemouth bass, Liu et al. reported that chronic hypoxia, combined with Cu^{2+} exposure, induced gill remodeling through endoplasmic reticulum stress, mitochondrial damage, and apoptosis pathways (Liu et al., 2023). In our study, TEM revealed that, compared to the normoxic group, prolonged hypoxic stress led to progressive fragmentation and dissipation of mitochondrial cristae in the gill cells of rainbow trout. Vacuoles that emerged at 24 h ruptured and disappeared by 48 h. Additionally, after 48 h of hypoxia, the nuclear membranes of gill cells ruptured and became wrinkled. These lesions were consistent with impaired energy supply and ionic transport under oxygen limitation, as suggested by the concurrent upregulation of glycolytic and redox programs. Structural and molecular changes converged, which was accompanied by apoptosis in the late phase during the 24 to 48 h interval.

Apoptosis is a programmed and orderly mode of cell death, serving as an active and adaptive response to environmental stressors (Milisav et al., 2017). In previous studies on *M. amblycephala*, hypoxia-exposed gills exhibited an increase in TUNEL-positive apoptotic fluorescence signals at days 4 and 7, accompanied by a significant rise in the apoptosis rate (Shuang et al., 2022). In the present study, the number of apoptotic cells in each treatment group was higher than in the control group. Moreover, as hypoxia duration increased, the apoptosis fluorescence ratio showed an upward trend. Additionally, apoptosis was accompanied by structural damage to the gill lamellae. This morphological change may reflect hypoxia-induced lamellar remodeling, which increases the respiratory surface area and reduces oxygen diffusion distance, thereby improving oxygen uptake efficiency (Nilsson, 2007; Zhou et al., 2023). Transcriptome analysis of gill cells revealed significant enrichment of DEGs in the apoptosis pathway in both DH0h vs.

DH24h and DH0h vs. DH48h comparisons. Notably, the pathway was downregulated at 24 h but upregulated at 48 h, indicating a shift from adaptive survival to irreversible damage. Prolonged hypoxia caused severe gill cell damage, triggering intensified apoptosis.

4.2. Hypoxia-induced oxidative stress responses in rainbow trout

In fish, hypoxic stress induces the excessive generation of ROS (Leonarduzzi et al., 2010), which exert toxic effects by causing DNA strand cleavage, triggering lipid peroxidation, and producing lipid peroxides (Tahmasbpour Marzony et al., 2016). Empirical evidence from multiple species demonstrates this phenomenon: ROS levels significantly increased in pacamã (*Lophiosilurus alexandri*) gills after 72-h hypoxia (Baldissera et al., 2020), in liver tissue of *Larimichthys polyactis* under varying hypoxic intensities (Wang et al., 2023), and progressively accumulated in *O. mykiss* gill cells during 24–48 h hypoxic exposure in our study. Concurrently, this oxidative challenge activates the antioxidant defense system, characterized by dynamic regulation of superoxide dismutase (SOD), catalase (CAT), and glutathione peroxidase (GPx) activities (Tan et al., 2016; Ding et al., 2023). In blunt snout bream, gill SOD activity rose with prolonged hypoxia while CAT maintained upward trends at 2.0 mg/L dissolved oxygen (Shuang et al., 2022). Small yellow croaker exhibited temporally differentiated responses — CAT activity peaked then declined (remaining elevated at 96 h), contrasting with SOD's sustained increase (Wang et al., 2023). Our observations in *O. mykiss* gills revealed coordinated yet temporally staggered responses: MDA (a lipid peroxidation biomarker) (Wilhelm Filho et al., 2005) accumulation paralleled progressive SOD elevation throughout 48-h hypoxia, while CAT activity peaked at 24 h before declining, though remaining above control levels. This CAT attenuation may reflect MDA-mediated enzyme inhibition (Zheng et al., 2021), as demonstrated in *Sebastes schlegelii* liver where hypoxia-induced MDA elevation correlated with oxidative stress intensification (Jia et al., 2023). These findings collectively suggested that antioxidant capacity under hypoxia was shaped by a dynamic balance between enzymatic defenses (SOD/CAT) and oxidative damage (MDA), with their temporal patterns indicative of species-specific strategies to maintain redox homeostasis. These biochemical trends were consistent with transcriptomic upregulation of glycolytic reprogramming and amino-acid biosynthesis, linking redox control to metabolic support.

4.3. Effects of hypoxic stress on glycolysis/gluconeogenesis pathway

KEGG enrichment showed upregulation at 24 h and 48 h, with stronger effects at 48 h; WGCNA (MEblue) converged on the same pathway. This consistent enrichment across DEGs and co-expression networks was consistent with ATP maintenance under oxygen limitation. The 24 to 48 h reinforcement of glycolytic signals suggested continued metabolic support as injury accumulated. In the PPI network, *pgk1* and *gapdhs* emerged as critical hub genes with high connectivity scores. *pgk1*, which catalyzes the ATP-generating step in glycolysis, was upregulated at both time points, highlighting its essential role in maintaining energy homeostasis (Wu et al., 2009). This aligns with studies in hybrid yellow catfish (*Pelteobagrus fulvidraco*♀ × *P. vachelli*♂), where *pgk1* showed hypoxia-induced upregulation in the brain and liver, followed by recovery upon reoxygenation (Pei et al., 2021). Similarly, GAPDHS functioned as a glycolytic enzyme and redox sensor via NAD^+/NADH interactions (Slivinskaya et al., 2022); its higher expression at 48 h may indicate roles in energy support and redox balance, as reported in *Carassius auratus* (Li et al., 2024a). WGCNA further highlighted additional key genes within the glycolysis/gluconeogenesis pathway (*hk1*, *pgm1*, *pgm2*, *pfklb*, *aldocb*, *gapdhs*, and *pgk1*) that were upregulated at 24 h and 48 h, with stronger effects at 48 h. These genes encode key glycolytic rate-limiting enzymes (HK1, PFKLB), intermediate metabolic enzymes involved in glucose metabolism (PGM1, PGM2), and enzymes with potential roles in both glycolysis and redox regulation (GAPDHS, PGK1). Similar upregulation has been reported in zebrafish (*Danio rerio*) (Dinarello et al., 2023) and common carp (*Cyprinus carpio*) (Li et al., 2024a), supporting a conserved pattern under hypoxia. Sustained elevation of *hk1* and *pfklb* was consistent with enhanced glucose phosphorylation and increased glycolytic flux (Huang et al., 2023). Upregulation of *pgm1* and *pgm2* may facilitate the interconversion of glucose-1-phosphate and glycogen, thereby routing substrates between glycogen turnover and glycolysis (Chen et al., 2024). Coordinated increases in *gapdhs* and *pgk1* may support ATP generation and help stabilize the NAD^+/NADH ratio (Pan et al., 2024). Collectively, these observations suggested a reinforced glycolytic program that supported energy supply while helping maintain metabolic homeostasis.

4.4. Effects of hypoxic stress on biosynthesis of amino acids

KEGG enrichment showed activation of the amino-acid biosynthesis pathway at 24 h and 48 h, with stronger effects at 48 h. WGCNA (MEblue) converged on the same signal, indicating agreement between differential expression and co-expression analyses. The PPI network identified *eprs1*, *yars*, and *eef2b* as hub genes, which are involved in aminoacyl-tRNA biosynthesis and translational elongation (Bogorad et al., 2018; Williams et al., 2019; Wu et al., 2020). Among these, EPRS1 catalyzed glutamic acid and proline charging to tRNA and may support the supply of precursors relevant to glutathione (GSH) metabolism under hypoxia (Dunning et al., 2013). EEF2B facilitated ribosomal translocation during translation elongation (Lang et al., 2002; Connolly et al., 2006), which may contribute to hypoxia-responsive protein synthesis. WGCNA highlighted coordinated upregulation of genes such as *aldocb*, *pgk1*, *pgam1a*, *bcat2*, *cbsb*, and *mat2aa*. Notably, *pgk1* and *aldocb*, which are traditionally associated with glycolysis, may have served as a metabolic bridge between carbohydrate and amino acid metabolism. Specifically, they contribute intermediates like 3-phosphoglycerate, which is crucial for serine biosynthesis. Serine, in turn, acts as a precursor for cysteine and glutathione (GSH), highlighting a potential link between glycolysis and antioxidant defense mechanisms under hypoxic conditions (Wang et al., 2020; Hahn et al., 2022). BCAT2 catalyzed the first step of branched-chain amino-acid catabolism, generating glutamate and branched-chain keto acids that can yield acetyl-CoA and other TCA inputs via downstream steps. These metabolites may support the tricarboxylic-acid (TCA) cycle under conditions of mitochondrial stress (Lei et al., 2020). Methionine cycling, facilitated by MAT2AA, produces S-adenosylmethionine (SAMe), a universal methyl donor central to epigenetic regulation and stress adaptation (Li et al., *2024b*). The sustained activation at 24 and 48 h of hypoxia was consistent with two complementary responses: (1) antioxidant buffering via GSH precursor synthesis to mitigate ROS damage, and (2) metabolic flexibility utilizing amino acids as alternative carbon sources when glycolytic supply was limited—a pattern also reported in hypoxia-tolerant species such as *Procambarus clarkii* (Lei et al., 2023).

4.5. Effects of hypoxic stress on steroid biosynthesis

Steroid biosynthesis was enriched only in the upregulated DEGs of DH0h vs 48 h, with no evident activation at 24 h. WGCNA (MEblue) converged on the same pathway. In the PPI network, *sec61a1* appeared as a hub gene. It facilitates cotranslational translocation of nascent secretory proteins—including enzymes of steroid biosynthesis (Itskanov and Park, 2023). Its upregulation at 48 h was consistent with enhanced endoplasmic reticulum (ER) activity, potentially relating to sterol pathway engagement under hypoxia. WGCNA highlighted coordinated upregulation of key genes (*fdft1*, *lss*, *tm7sf2*, *dhcr7*, and *dhcr24*) in the MEblue module. FDFT1 catalyzed the conversion of farnesyl pyrophosphate to squalene, committing the first step in cholesterol biosynthesis (Coman et al., 2018). DHCR24 catalyzed a terminal reduction in sterol synthesis and has been implicated in redox regulation via its thioredoxin-like domain (Zerenturk et al., 2013). The gradual increase

in the expression of these genes from 24 to 48 h of hypoxia may reflect two potential physiological demands. Together, these data delineate a 48 h-restricted, late-phase transcriptional engagement of the sterol biosynthetic machinery under hypoxia, with no evidence at 24 h. This time-dependent pattern was consistent with staged responses described in gill biology (Hochachka and Somero, 2002). Such late-phase activation may reflect compensatory membrane repair or corticosteroid-mediated stress adaptation. However, functional validation is still required.

4.6. Effects of hypoxic stress on apoptosis

KEGG enrichment indicated biphasic regulation of the apoptosis pathway under hypoxia, with downregulation at 24 h and upregulation at 48 h; WGCNA (MEblue) converged on the same pattern. This profile was consistent with a transient suppression of apoptosis at 24 h, potentially supporting energy conservation and short-term cell survival. By 48 h, prolonged hypoxia was associated with activation of programmed cell death, potentially facilitating the removal of irreversibly damaged cells (Richards, 2009). This stage-dependent pattern suggested regulated control over cell-survival versus cell-death programs during hypoxia. At 48 h, the expression profile included decreased *bcl2l1* and increased *casp6a* and *map3k5*, together with changes in *map2k2a*, which was consistent with activation of apoptotic and stress-responsive signaling (Ichijo et al., 1997). These transcriptional changes aligned with TEM evidence of progressive mitochondrial cristae disruption, a hallmark of commitment to apoptosis (Scorrano et al., 2002).

5. Conclusion

In summary, rainbow trout exhibited a staged response to hypoxic stress. At 24 h, metabolic reprogramming and antioxidant activation maintained cellular homeostasis, whereas at 48 h, prolonged hypoxia led to severe structural damage, apoptosis induction, and upregulation of steroid biosynthesis. These findings provide new insights into the temporal regulation of hypoxia adaptation in rainbow trout and highlight potential molecular markers and time windows for managing hypoxia in aquaculture.

CRediT authorship contribution statement

Ziyi Zhao: Writing – original draft, Software, Methodology, Investigation. **Mengqun Liu:** Resources, Data curation. **Qiusheng Wang:** Investigation, Data curation. **Haishen Wen:** Writing – review & editing, Resources, Funding acquisition, Conceptualization. **Xin Qi:** Writing – review & editing, Methodology, Conceptualization.

Declaration of competing interest

The authors declare that they have no conflict of interest. All authors have approved the final version of this manuscript and agree to be accountable for all aspects of the work.

Acknowledgments

This work was supported by the National Natural Science Foundation of China [3217210108] and Shandong Provincial Key Research and Development Program-Major Scientific and Technological Innovation Project [2022ZLGX01].

Appendix A. Supplementary data

Supplementary data to this article can be found online at https://doi.org/10.1016/j.cbd.2025.101672.

Data availability

I have submitted my data on NCBI , the project number is PRJNA1270413

References

Aksakal, E., Soydan, E., Tunç, A., Vural, O., Kamaszewski, M., Ekinci, D., 2023. Chronic hypoxia and hyperoxia alter tissue-specific fatty acid profile and FD6D and elongase gene expression levels in rainbow trout (*Oncorhynchus mykiss*). J. Comp. Physiol. B. 193, 401–412.

Baldissera, M.D., De Freitas Souza, C., Boaventura, T.P., Nakayama, C.L., Baldisserotto, B., Luz, R.K., 2020. Involvement of the phosphoryl transfer network in gill bioenergetic imbalance of pacamã (*Lophiosilurus alexandri*) subjected to hypoxia: notable participation of creatine kinase. Fish Physiol. Biochem. 46, 405–416.

Bogorad, A.M., Lin, K.Y., Marintchev, A., 2018. eIF2B mechanisms of action and regulation: a thermodynamic view. Biochemistry 57, 1426–1435.

Bolger, A.M., Lohse, M., Usadel, B., 2014. Trimmomatic: a flexible trimmer for illumina sequence data. Bioinformatics 30, 2114–2120.

Brauner, C.J., Rombough, P.J., 2012. Ontogeny and paleophysiology of the gill: new insights from larval and air-breathing fish. Respir. Physiol. Neurobiol. 184, 293–300.

Cappello, T., Maisano, M., Giannetto, A., Parrino, V., Mauceri, A., Fasulo, S., 2015. Neurotoxicological effects on marine mussel *Mytilus galloprovincialis* caged at petrochemical contaminated areas (eastern Sicily, Italy): ^{1}H NMR and immunohistochemical assays. Comp. Biochem. Physiol. C Toxicol. Pharmacol. 169, 7–15.

Chen, C.-C., Gong, G.-C., Shiah, F.-K., 2007. Hypoxia in the East China Sea: one of the largest coastal low-oxygen areas in the world. Mar. Environ. Res. 64, 399–408.

Chen, F., Ling, X., Zhao, Y., Fu, S., 2022. Hypoxia-induced oxidative stress and apoptosis in gills of scaleless carp (*Gymnocypris przewalskii*). Fish Physiol. Biochem. 48, 911–924.

Chen, J., Zhou, Y., Liu, Z., Lu, Y., Jiang, Y., Cao, K., Zhou, N., Wang, D., Zhang, C., Zhou, N., Shi, K., Zhang, L., Zhou, L., Wang, Z., Zhang, H., Tang, K., Ma, J., Lv, J., Huang, B., 2024. Hepatic glycogenesis antagonizes lipogenesis by blocking S1P via UDPG. Science 383, eadi3332.

Cheng, C.-H., Guo, Z.-X., Luo, S.-W., Wang, A.-L., 2018. Effects of high temperature on biochemical parameters, oxidative stress, DNA damage and apoptosis of pufferfish (*Takifugu obscurus*). Ecotoxicol. Environ. Saf. 150, 190–198.

Chin, C.-H., Chen, S.-H., Wu, H.-H., Ho, C.-W., Ko, M.-T., Lin, C.-Y., 2014. CytoHubba: identifying hub objects and sub-networks from complex interactome. BMC Syst. Biol. 8 (S11).

Coman, D., Vissers, L.E.L.M., Riley, L.G., Kwint, M.P., Hauck, R., Koster, J., Geuer, S., Hopkins, S., Hallinan, B., Sweetman, L., Engelke, U.F.H., Burrow, T.A., Cardinal, J., McGill, J., Inwood, A., Gurnsey, C., Waterham, H.R., Christodoulou, J., Wevers, R.A., Pitt, J., 2018. Squalene synthase deficiency: clinical, biochemical, and molecular characterization of a defect in cholesterol biosynthesis. Am. J. Hum. Genet. 103, 125–130.

Connolly, E., Braunstein, S., Formenti, S., Schneider, R.J., 2006. Hypoxia inhibits protein synthesis through a 4E-BP1 and elongation factor 2 kinase pathway controlled by mTOR and uncoupled in breast cancer cells. Mol. Cell. Biol. 26, 3955–3965.

Dinarello, A., Betto, R.M., Diamante, L., Tesoriere, A., Ghirardo, R., Cioccarelli, C., Meneghetti, G., Peron, M., Laquatra, C., Tiso, N., Martello, G., Argenton, F., 2023. STAT3 and HIF1α cooperatively mediate the transcriptional and physiological responses to hypoxia. Cell Death Dis. 9, 226.

Ding, W., Cao, L., Cao, Z., Bing, X., 2023. Transcriptomic responses of the liver of mandarin fish (*Siniperca chuatsi*) under hypoxic stress. J. Fish Biol. 103, 44–58.

Dunning, S., Ur Rehman, A., Tiebosch, M.H., Hannivoort, R.A., Haijer, F.W., Woudenberg, J., Van Den Heuvel, F.A.J., Buist-Homan, M., Faber, K.N., Moshage, H., 2013. Glutathione and antioxidant enzymes serve complementary roles in protecting activated hepatic stellate cells against hydrogen peroxide-induced cell death. Biochim. Biophys. Acta (BBA) Mol. Basis Dis. 1832, 2027–2034.

Feng, J., Guo, Y., Gao, Y., Zhu, L., 2016. Effects of hypoxia on the physiology of zebrafish (*Danio rerio*): initial responses, acclimation and recovery. Bull. Environ. Contam. Toxicol. 96, 43–48.

Gill, N., Dhillon, B., 2022. RNA-seq data analysis for differential expression *Fusarium wilt*. In: Coleman, J. (Ed.), Methods in Molecular Biology, vol. 2391. Springer US, New York, NY, pp. 45–54.

Hahn, K.R., Kwon, H.J., Yoon, Y.S., Kim, D.W., Hwang, I.K., 2022. Phosphoglycerate kinase 1 protects against ischemic damage in the gerbil hippocampus. Aging 14, 8886–8899.

Harper, C., Wolf, J.C., 2009. Morphologic effects of the stress response in fish. ILAR J. 50, 387–396.

He, L., Eslamfam, S., Ma, X., Li, D., 2016. Autophagy and the nutritional signaling pathway. Front. Agric. Sci. Eng. 3, 222.

Hochachka, P.W., Somero, G.N., 2002. Biochemical Adaptation: Mechanism and Process in Physiological Evolution. Oxford University Press, New York.

Hou, Z.-S., Wen, H.-S., Li, J.-F., He, F., Li, Y., Qi, X., 2020. Environmental hypoxia causes growth retardation, osteoclast differentiation and calcium dyshomeostasis in juvenile rainbow trout (*Oncorhynchus mykiss*). Sci. Total Environ. 705, 135272.

Huang, K.-J., Feng, L., Wu, P., Liu, Y., Zhang, L., Mi, H.-F., Zhou, X.-Q., Jiang, W.-D., 2024. Hypoxia leads to gill endoplasmic reticulum stress and disruption of mitochondrial homeostasis in grass carp (*Ctenopharyngodon idella*): mitigation effect of thiamine. J. Hazard. Mater. 469, 134005.

Huang, Z.-W., Zhang, X.-N., Zhang, L., Liu, L.-L., Zhang, J.-W., Sun, Y.-X., Xu, J.-Q., Liu, Q., Long, Z.-J., 2023. STAT5 promotes PD-L1 expression by facilitating histone lactylation to drive immunosuppression in acute myeloid leukemia. Sig. Transduct. Target. Ther. 8, 391.
Ichijo, H., Nishida, E., Irie, K., ten Dijke, P., Saitoh, M., Moriguchi, T., Takagi, M., Matsumoto, K., Miyazono, K., Gotoh, Y., 1997. Induction of apoptosis by ASK1, a mammalian MAPKKK that activates SAPK/JNK and p38 signaling pathways. Science 275, 90–94.
Itskanov, S., Park, E., 2023. Mechanism of protein translocation by the Sec61 translocon complex. Cold Spring Harb. Perspect. Biol. 15, a041250.
Jia, Y., Wang, F., Gao, Y., Qin, H., Guan, C., 2023. Hypoxia stress induces hepatic antioxidant activity and apoptosis, but stimulates immune response and immune-related gene expression in black rockfish *Sebastes schlegelii*. Aquat. Toxicol. 258, 106502.
Lang, KJD, Kappel, A, Goodall, G.J., 2002. Hypoxia-inducible factor-1 mRNA contains an internal ribosome entry site that allows efficient translation during normoxia and hypoxia. Mol. Cell. Biol. 13, 1792–1801.
Langfelder, P., Horvath, S., 2008. WGCNA: an R package for weighted correlation network analysis. BMC Bioinformatics 9, 559.
Lei, M.-Z., Li, X.-X., Zhang, Y., Li, J.-T., Zhang, F., Wang, Y.-P., Yin, M., Qu, J., Lei, Q.-Y., 2020. Acetylation promotes BCAT2 degradation to suppress BCAA catabolism and pancreatic cancer growth. Sig. Transduct. Target. Ther. 5, 70.
Lei, Y., Gao, Y., Li, X., Luo, X., Wang, L., Wu, W., Xiong, G., Chu, S., Li, S., 2023. Integrating transcriptomic and proteomics revealed the response mechanism of red swamp crayfish (*Procambarus clarkii*) muscle under cold stress. Food Sci. Anim. Prod. 1, 9240007.
Leonarduzzi, G., Sottero, B., Poli, G., 2010. Targeting tissue oxidative damage by means of cell signaling modulators: the antioxidant concept revisited. Pharmacol. Ther. 128, 336–374.
Li, F., Liu, P., Mi, W., Li, L., Anderson, N.M., Lesner, N.P., Burrows, M., Plesset, J., Majer, A., Wang, G., Li, J., Zhu, L., Keith, B., Simon, M.C., 2024b. Blocking methionine catabolism induces senescence and confers vulnerability to GSK3 inhibition in liver cancer. Nat. Can. 5, 131–146.
Li, Y., Wu, S., Huang, J., Zhao, L., 2024a. Integration of physiological, miRNA-mRNA interaction and functional analysis reveals the molecular mechanism underlying hypoxia stress tolerance in crucian carp (*Carassius auratus*). FASEB J. 38, e23722.
Liang, G., Fu, W., Wang, K., 2019. Analysis of *t*-test misuses and SPSS operations in medical research papers. Burns Trauma 7, s41038-019-0170-3.
Liao, Y., Smyth, G.K., Shi, W., 2014. featureCounts: an efficient general purpose program for assigning sequence reads to genomic features. Bioinformatics 30, 923–930.
Liu, Q., Wang, H., Ge, J., Li, L., Luo, J., He, K., Yan, H., Zhang, X., Tahir, R., Luo, W., Chen, S., Cheng, Z., Zhao, L., Yang, S., 2023. Chronic hypoxia and Cu^{2+} exposure induce gill remodeling of largemouth bass through endoplasmic reticulum stress, mitochondrial damage and apoptosis. Aquat. Toxicol. 255, 106373.
Livak, K.J., Schmittgen, T.D., 2001. Analysis of relative gene expression data using real-time quantitative PCR and the $2^{-\Delta\Delta CT}$ method. Methods 25, 402–408.
Matey, V., Iftikar, F.I., De Boeck, G., Scott, G.R., Sloman, K.A., Almeida-Val, V.M.F., Val, A.L., Wood, C.M., 2011. Gill morphology and acute hypoxia: responses of mitochondria-rich, pavement, and mucous cells in the Amazonian Oscar (*Astronotus ocellatus*) and the rainbow trout (*Oncorhynchus mykiss*), two species with very different approaches to the osmo-respiratory compromise. Can. J. Zool. 89, 307–324.
Milisav, I., Poljšak, B., Ribarič, S., 2017. Reduced risk of apoptosis: mechanisms of stress responses. Apoptosis 22, 265–283.
Mruk, D.D., Silvestrini, B., Mo, M., Cheng, C.Y., 2002. Antioxidant superoxide dismutase — a review: its function, regulation in the testis, and role in male fertility. Contraception 65, 305–311.
Mu, Y., Li, W., Wei, Z., He, L., Zhang, W., Chen, X., 2020. Transcriptome analysis reveals molecular strategies in gills and heart of large yellow croaker (*Larimichthys crocea*) under hypoxia stress. Fish Shellfish Immunol. 104, 304–313.
Nilsson, G.E., 2007. Gill remodeling in fish — a new fashion or an ancient secret? J. Exp. Biol. 210, 2403–2409.
Pan, Y., Zhou, Y., Shen, Y., Xu, L., Liu, H., Zhang, N., Huang, T., Meng, K., Liu, Y., Wang, L., Bai, G., Chen, Q., Zhu, Y., Zou, X., Wang, S., Wang, Z., Wang, L., 2024. Hypoxia stimulates PYGB enzymatic activity to promote glycogen metabolism and cholangiocarcinoma progression. Cancer Res. 84, 3803–3817.
Pan, Y.K., Perry, S.F., 2020. Neuroendocrine control of breathing in fish. Mol. Cell. Endocrinol. 509, 110800.
Pei, X., Chu, M., Tang, P., Zhang, H., Zhang, X., Zheng, X., Li, J., Mei, J., Wang, T., Yin, S., 2021. Effects of acute hypoxia and reoxygenation on oxygen sensors, respiratory metabolism, oxidative stress, and apoptosis in hybrid yellow catfish "huangyou-1". Fish Physiol. Biochem. 47, 1429–1448.
Peivandi, Z., Shirazi, F.H., Teimourian, S., Farnam, G., Babaei, V., Mehrparvar, N., Koohsari, N., Ashtarinezhad, A., 2024. Silica nanoparticles-induced cytotoxicity and genotoxicity in A549 cell lines. Sci. Rep. 14, 14484.
Pertea, M., Pertea, G.M., Antonescu, C.M., Chang, T.-C., Mendell, J.T., Salzberg, S.L., 2015. StringTie enables improved reconstruction of a transcriptome from RNA-seq reads. Nat. Biotechnol. 33, 290–295.
Qiang, J., Yang, H., Wang, H., Kpundeh, M.D., Xu, P., 2013. Interacting effects of water temperature and dietary protein level on hematological parameters in Nile tilapia juveniles, *Oreochromis niloticus* (L.) and mortality under *Streptococcus iniae* infection. Fish Shellfish Immunol. 34, 8–16.
Richards, J.G., Farrell, A.P., Brauner, C.J., 2009. Chapter 10 Metabolic and molecular responses of fish to hypoxia. In: Richards, J.G. (Ed.), Fish Physiology Hypoxia, vol. 27. Academic Press, pp. 443–485.
Roesner, A, Hankeln, T, Burmester, T, 2006. Hypoxia induces a complex response of globin expression in zebrafish (*Danio rerio*). J. Exp. Biol. 209 (Pt 11), 2129–2137.
Rombough, P., 2007. The functional ontogeny of the teleost gill: which comes first, gas or ion exchange? Comp. Biochem. Physiol. A Mol. Integr. Physiol. 148, 732–742.
Saetan, W., Tian, C., Yu, J., Lin, X., He, F., Huang, Y., Shi, H., Zhang, Y., Li, G., 2020. Comparative transcriptome analysis of gill tissue in response to hypoxia in silver sillago (*Sillago sihama*). Animals 10, 628.
Schneider, C.A., Rasband, W.S., Eliceiri, K.W., 2012. NIH image to ImageJ: 25 years of image analysis. Nat. Methods 9, 671–675.
Schulte, P.M., 2015. The effects of temperature on aerobic metabolism: towards a mechanistic understanding of the responses of ectotherms to a changing environment. ed J E Podrabsky, J H Stillman and L Tomanek J. Exp. Biol. 218, 1856–1866.
Scorrano, L., Ashiya, M., Buttle, K., Weiler, S., Oakes, S.A., Mannella, C.A., Korsmeyer, S. J., 2002. A distinct pathway remodels mitochondrial cristae and mobilizes cytochrome c during apoptosis. Dev. Cell 2, 55–67.
Shang, F., Bao, M., Liu, F., Hu, Z., Wang, S., Yang, X., Yu, Y., Zhang, H., Jiang, C., Qiu, X., Liu, Y., Wang, X., 2022. Transcriptome profiling of tiger pufferfish (*Takifugu rubripes*) gills in response to acute hypoxia. Aquaculture 557, 738324.
Shannon, P., Markiel, A., Ozier, O., Baliga, N.S., Wang, J.T., Ramage, D., Amin, N., Schwikowski, B., Ideker, T., 2003. Cytoscape: a software environment for integrated models of biomolecular interaction networks. Genome Res. 13, 2498–2504.
Shuang, L., Su, X., Zheng, G., Zou, S., 2022. Effects of hypoxia and reoxygenation on gill remodeling, apoptosis, and oxidative stress in hypoxia-tolerant new variety blunt snout bream (*Megalobrama amblycephala*). Fish Physiol. Biochem. 48, 263–274.
Slivinskaya, E.A., Plekhanova, N.S., Altman, I.B., Yampolskaya, T.A., 2022. Engineering of *Escherichia coli* glyceraldehyde-3-phosphate dehydrogenase with dual NAD^+/$NADP^+$ cofactor specificity for improving amino acid production. Microorganisms 10, 976.
Sollid, J., Kjernsli, A., De Angelis, P.M., Røhr, Å.K., Nilsson, G.E., 2005. Cell proliferation and gill morphology in anoxic crucian carp. Am. J. Phys. Regul. Integr. Comp. Phys. 289, R1196–R1201.
Song, Z., Ye, W., Tao, Y., Zheng, T., Qiang, J., Li, Y., Liu, W., Xu, P., 2022. Transcriptome and 16S rRNA analyses reveal that hypoxic stress affects the antioxidant capacity of largemouth bass (*Micropterus salmoides*), resulting in intestinal tissue damage and structural changes in microflora. Antioxidants 12, 1.
Stierhoff, K.L., Targett, T.E., Grecay, P.A., 2003. Hypoxia tolerance of the mummichog: the role of access to the water surface. J. Fish Biol. 63, 580–592.
Stramma, L., Johnson, G.C., Sprintall, J., Mohrholz, V., 2008. Expanding oxygen-minimum zones in the tropical oceans. Science 320, 655–658.
Sun, J.L., Zhao, L.L., Wu, H., Liu, Q., Liao, L., Luo, J., Lian, W.Q., Cui, C., Jin, L., Ma, J.D., Li, M.Z., Yang, S., 2020. Acute hypoxia changes the mode of glucose and lipid utilization in the liver of the largemouth bass (*Micropterus salmoides*). Sci. Total Environ. 713, 135157.
Tahmasbpour Marzony, E., Nejad-Moghadam, A., Ghanei, M., Panahi, Y., 2016. Sulfur mustard causes oxidants/antioxidants imbalance through the overexpression of free radical producing-related genes in human mustard lungs. Environ. Toxicol. Pharmacol. 45, 187–192.
Tan, P., Wang, Y.-J., Li, S., Wang, Y., He, J.-Y., Chen, Y.-Y., Deng, H.-Q., Huang, W., Zhan, J.-K., Liu, Y.-S., 2016. The PI3K/akt/mTOR pathway regulates the replicative senescence of human VSMCs. Mol. Cell. Biochem. 422, 1–10.
Tran-Duy, A., Schrama, J.W., Van Dam, A.A., Verreth, J.A.J., 2008. Effects of oxygen concentration and body weight on maximum feed intake, growth and hematological parameters of Nile tilapia, *Oreochromis niloticus*. Aquaculture 275, 152–162.
Wang, H., Cui, L., Li, D., Fan, M., Liu, Z., Liu, C., Pan, S., Zhang, L., Zhang, H., Zhao, Y., 2020. Overexpression of *PSAT1* regulated by G9A sustains cell proliferation in colorectal cancer. Sig. Transduct. Target. Ther. 5, 47.
Wang, J., Wang, L., Liu, Y., Du, C., Hou, C., Xie, Q., Tang, D., Liu, F., Lou, B., Zhu, J., 2023. Change to the transcriptomic profile, oxidative stress, apoptotic and immunity in the liver of small yellow croaker (*Larimichthys polyactis*) under hypoxic stress. Aquaculture 576, 739854.
Wang, P., Liu, H., Zhao, S., Yu, S., Xie, S., Hua, S., Yan, B., Xing, C., Gao, H., 2022. Hypoxia stress affects the physiological responses, apoptosis and innate immunity of Kuruma shrimp, *Marsupenaeus japonicus*. Fish Shellfish Immunol. 122, 206–214.
Ward, C.M., Tos, T.-H., Pederson, S.M., 2020. ngsReports: a bioconductor package for managing FastQC reports and other NGS related log files. ed J Hancock Bioinformatics 36, 2587–2588.
Wilhelm Filho, D., Torres, M.A., Zaniboni-Filho, E., Pedrosa, R.C., 2005. Effect of different oxygen tensions on weight gain, feed conversion, and antioxidant status in piapara, *Leporinus elongatus* (Valenciennes, 1847). Aquaculture 244, 349–357.
Williams, K.B., Brigatti, K.W., Puffenberger, E.G., Gonzaga-Jauregui, C., Griffin, L.B., Martinez, E.D., Wenger, O.K., Yoder, M.A., Kandula, V.V.R., Fox, M.D., Demczko, M. M., Poskitt, L., Furuya, K.N., Reid, J.G., Overton, J.D., Baras, A., Miles, L., Radhakrishnan, K., Carson, V.J., Antonellis, A., Jinks, R.N., Strauss, K.A., 2019. Homozygosity for a mutation affecting the catalytic domain of tyrosyl-tRNA synthetase (YARS) causes multisystem disease. Hum. Mol. Genet. 28, 525–538.
Wu, J., Subbaiah, K.C.V., Xie, L.H., Jiang, F., Khor, E.-S., Mickelsen, D., Myers, J.R., Tang, W.H.W., Yao, P., 2020. Glutamyl-prolyl-tRNA synthetase regulates proline-rich pro-fibrotic protein synthesis during cardiac fibrosis. Circ. Res. 127, 827–846.
Wu, S., Storey, J.M., Storey, K.B., 2009. Phosphoglycerate kinase 1 expression responds to freezing, anoxia, and dehydration stresses in the freeze tolerant wood frog, *Rana sylvatica*. J. Exp. Zool. 311A, 57–67.
Xing, M., Rong, Z., Zhao, X., Gao, X., Hou, Z., Zhang, L., Khor, W., Xu, Y., Chen, L., Wu, C., 2025. Transcriptome analysis reveals hypoxic response key genes and modules as well as adaptive mechanism of crucian carp (*Carassius auratus*) gill under hypoxic stress. Front. Immunol. 16, 1543605.
Yang, S., Yan, T., Wu, H., Xiao, Q., Fu, H.M., Luo, J., Zhou, J., Zhao, L.L., Wang, Y., Yang, S.Y., Sun, J.L., Ye, X., Li, S.J., 2017. Acute hypoxic stress: effect on blood

parameters, antioxidant enzymes, and expression of HIF-1alpha and GLUT-1 genes in largemouth bass (*Micropterus salmoides*). Fish Shellfish Immunol. 67, 449–458.
Zelko, I.N., Mariani, T.J., Folz, R.J., 2002. Superoxide dismutase multigene family: a comparison of the CuZn-SOD (SOD1), Mn-SOD (SOD2), and EC-SOD (SOD3) gene structures, evolution, and expression. Free Radic. Biol. Med. 33, 337–349.
Zerenturk, E.J., Sharpe, L.J., Ikonen, E., Brown, A.J., 2013. Desmosterol and DHCR24: unexpected new directions for a terminal step in cholesterol synthesis. Prog. Lipid Res. 52, 666–680.
Zhang, H., Li, R., Wang, Y., Zhou, J., Xu, H., Gou, M., Ye, J., Qiu, X., Wang, X., 2023. Transcriptomic analysis of *Takifugu obscurus* gills under acute hypoxic stress. Animals 13, 1572.
Zheng, X., Fu, D., Cheng, J., Tang, R., Chu, M., Chu, P., Wang, T., Yin, S., 2021. Effects of hypoxic stress and recovery on oxidative stress, apoptosis, and intestinal microorganisms in *Pelteobagrus vachelli*. Aquaculture 543, 736945.
Zhou, H., Jiang, Y., Xu, Y., Cui, A., Feng, Y., Jin, Z., Wang, B., 2023. Histological, microecological and transcriptomic physiological responses underlying hypoxia and reoxygenation adaptation in yellowtail kingfish (*Seriola lalandi*). Front. Mar. Sci. 10.